Europium(III) Luminescence and Tyrosine to Terbium(III) Energy-Transfer Studies of Invertebrate (Octopus) Calmodulin†

JoAnne Bruno,‡ William DeW. Horrocks, Jr.,*,‡ and Randy J. Zauhar§

Department of Chemistry and Department of Molecular and Cell Biology, The Pennsylvania State University, University Park, Pennsylvania 16802

Received February 13, 1992; Revised Manuscript Received May 1, 1992

ABSTRACT: The effects of minor differences in the amino acid sequences between a vertebrate (bovine testes) and an invertebrate (octopus) calmodulin on metal ion binding were investigated via laser-induced Eu^{3+} and Tb^{3+} luminescence. Amino acid substitutions at residues which are coordinated to the metal ion do not produce any detectable changes in the $^7F_0 \rightarrow {}^5D_0$ excitation spectrum of the Eu^{3+} ion bound to octopus calmodulin relative to bovine testes calmodulin; only minor differences in the excited-state lifetime values in D_2O solution are observed. The dissociation constants for Eu^{3+} (1.0 ± 0.2 μM) and Tb^{3+} (5 ± 1 μM) from the weak lanthanide binding sites (III and IV, numbered from the amino terminus) of octopus calmodulin were measured using luminescence techniques. Both values agree well with those reported previously for bovine testes calmodulin [Mulqueen, P. M., Tingey, J. M., & Horrocks, W. D., Jr. (1985) *Biochemistry 24*, 6639–6645]. The measured dissociation constant of Eu^{3+} bound in the tight lanthanide binding sites (I and II) is 6 ± 2 nM for octopus calmodulin and 12 ± 2 nM for bovine testes calmodulin. The distances between sites I and II (12.4 ± 0.5 Å) and sites III and IV (11.7 ± 0.8 Å) were determined from Förster-type energy transfer in D_2O solutions of octopus calmodulin containing bound Eu^{3+} donor and Nd^{3+} acceptor ions. Förster theory parameters for nonradiative energy transfer between Tyr138 and Tb^{3+} ions bound at sites III and IV of octopus calmodulin were comprehensively evaluated, including a dynamics simulation of the orientation factor κ^2. This theory is found to account quantitatively for the observed energy-transfer efficiency as evaluated from the observed sensitized Tb^{3+} emission.

Calmodulin (CaM)[1] is a small (M_r = 16 790), heat-stable, acidic (pI = 3.9–4.3) protein found in prokaryotic and eukaryotic cells where its function is to mediate rapid, transient increases in intracellular calcium concentration and thereby modulate the action of various enzymes [for recent reviews, see Hidaka (1989) and Gerday et al. (1988)]. The three-dimensional structure (Babu et al., 1988, 1985) indicates that calmodulin is dumbbell-like in shape with a long central helix connecting two globular lobes, each containing two metal binding sites. There are four EF-hand (Kretsinger et al., 1973) calcium binding loops. The binding of calcium to calmodulin is a sequential process, with binding occurring initially at two high-affinity sites (domains III and IV, numbered from the amino terminus), followed by binding at two low-affinity sites (domains I and II; Wang, 1985; Wang et al., 1984, 1982; Crouch & Klee, 1980). An examination of the amino acid sequences of calmodulins from numerous sources reveals high homology among calmodulin isotypes and strongly suggests a common ancestor for this important protein. The amino acid sequences of 6 higher animals differ in only 7 positions out of 148 residues, 3 of which reflect differences in amide assignment. Domain I (residues 9–42) is entirely conserved, and only one substitution (Asn60→Asp) is observed in domain II (residues 45–78). The greatest variability in the primary sequence occurs in domain III (Asn97→Asp; Tyr99→Phe) and domain IV (Asn129→Asp), as well as at positions 143 and 147 outside of binding loop IV [for a review, see Smith et al. (1987)]. However, many of the substitutions are conservative, such as the Tyr→Phe change at position 99, which is seen for all invertebrate calmodulins.

The invertebrate calmodulin from octopus (OCaM), by analogy with scallop calmodulin, varies from the vertebrate protein at three to six positions: Asn60→Asp, Asn97→Asp, Tyr99→Phe, Asn129→Asp, Gln143→Thr, and Ala147→Ser (Toda et al., 1981), depending on the amide assignments of the vertebrate source used in the comparison. From the latest refinement of the X-ray crystal structure of rat testis calmodulin (Babu et al., 1988), it is known that the amide oxygen of the asparagine side chain of residues 60 and 97 (loops II and III, respectively), as well as the backbone carbonyl oxygen of Tyr99 (loop III), coordinates to the metal ion. The substitutions in the second and third metal binding loops are conservative. The remaining two differences in the sequence, at positions 143 and 147, lie outside of the fourth metal binding loop.

Studies which probe the protein-bound metal ion are invaluable in determining the role of the metal ion in the structure and function of the protein. The ability of certain lanthanide ions to luminesce at room temperature and their chemical similarity to the spectroscopically silent calcium ion has made them a widely used probe species for the study of calcium binding proteins (Horrocks, 1982; Horrocks & Sudnick, 1981; Reuben, 1979). Although it has been shown that the binding order is reversed (from calcium) for lanthanide ions (domains I and II are the high-affinity sites; domains III

† This work was supported by U.S. Public Health Service Grant GM23599 from the National Institutes of Health.

* Author to whom correspondence should be addressed.

‡ Department of Chemistry.

§ Department of Molecular and Cell Biology and The Biotechnology Institute.

[1] Abbreviations: CaM, calmodulin; OCaM, octopus calmodulin; BCaM, bovine testes calmodulin; DmCaM, *Drosophila melanogaster* calmodulin; MWCO, molecular weight cutoff; RMS, root mean square; Hepes, *N*-(2-hydroxyethyl)piperazine-*N*′-2-ethanesulfonic acid; fwhm, full width at half-maximum; dpa, 2,6-pyridinedicarboxylic acid; dtpa, diethylenetriaminepentaacetic acid; edta, ethylenediaminetetraacetic acid; egta, ethylene glycol bis(β-aminoethyl ether)-*N*,*N*,*N*′,*N*′-tetraacetic acid; hedta, *N*-(2-hydroxyethyl)ethylenediaminetriacetic acid; ttha, triethylenetetraaminehexaacetic acid.

0006-2960/92/0431-7016$03.00/0

and IV are the low-affinity sites; Martin et al., 1985; Wang et al., 1984; Andersson et al., 1983), Ln^{3+}-bound calmodulin activates the camodulin-dependent enzyme phosphodiesterase to levels comparable to those achieved by the Ca^{2+}-bound protein (Buccigross et al., 1989; Chao et al., 1984). Excitation spectroscopy of the $^7F_0 \rightarrow {}^5D_0$ transition of Eu^{3+} ions bound to bovine testes calmodulin (BCaM) has provided a wealth of information regarding the metal ion binding characteristics of this protein (Horrocks & Tingey, 1988; Mulqueen et al., 1985). In our earlier studies, we were able to identify three distinct spectroscopic classes of metal ion binding site, count the number of water molecules coordinated to each class of metal ion, and measure the distance separating the metal binding sites in each lobe. These same techniques are applied by us in the present investigation of the invertebrate calmodulin derived from octopus to discern if any metal binding or spectroscopic differences arise from subtle substitutions in the amino acid sequences of vertebrate and invertebrate calmodulins.

In addition, the present research exploits the natural Tyr→Phe mutation at position 99 in quantitating the energy transfer between the remaining fluorescent tyrosine residue, Tyr138, and protein-bound Tb^{3+} ions. Tyrosine to Tb^{3+} radiationless energy transfer, thought to occur via the Förster dipole–dipole mechanism (Förster, 1948), has been investigated previously (Eberspach et al., 1988) using the Tyr48 on Pike II parvalbumin and Tb^{3+} ions bound at the CD and EF sites. However, the measured distances between the chromophore and the metal ions did not agree well with distances estimated from the X-ray crystal structure (Kumar et al., 1990; Moews & Kretsinger, 1975). Here we present a thorough analysis of the parameters which describe Förster energy transfer between tyrosine and Tb^{3+} ions and provide proof that the nonradiative energy transfer observed in OCaM occurs by this mechanism.

MATERIALS AND METHODS

Materials. All chemicals were of the highest grade commercially available. Triply distilled water that had been passed over a deionizing column was used throughout. In order to reduce metal ion contamination, only acid-washed glassware and plasticware were used. All calmodulin solutions were buffered (0.05 M Hepes, pH or pD 7.0) and made 0.5 M in KCl to avoid nonspecific Ln^{3+} ion binding and the resulting precipitation that occurs at lower salt concentrations. $EuCl_3 \cdot 6H_2O$, $TbCl_3 \cdot 6H_2O$, and $CaCl_2 \cdot 6H_2O$ were obtained from Aldrich Chemical Co., and were used without further purification. All metal ion solutions were standardized by a complexometric technique (Fritz et al., 1958).

Calmodulin Preparation. Frozen octopus was obtained from a local supermarket, and the calmodulin was purified from skinned tissue using a method set forth in detail in an earlier paper (Mulqueen et al., 1985). Edta was removed from calmodulin via diafiltration on an Amicon 8200 stirred cell equipped with a YM10 membrane (MWCO 10K). Two equivalents of sodium acetate was added initially to the protein solution which was then concentrated 3-fold and rediluted with 0.05 M Hepes buffer at 4 °C. This procedure was repeated until the residual edta concentration had been reduced to less than 0.05 equiv. Edta contamination was monitored by the magnitude of the eluent absorbance at 248 nm and by a final check of the protein sample using the laser-induced Eu^{3+} luminescence method described previously (Mulqueen et al., 1985). The purified calmodulin was kept frozen in the same buffered solution at −20 °C until needed. Protein purity was evaluated by SDS–PAGE on 20% acrylamide gels stained with a combined Coomassie Blue–Silver Stain procedure (DeMoreno et al., 1985). Typical protein yields were 5–6 mg/kg wet tissue. The concentration of calmodulin was determined using both the absorbance at 278 nm ($\epsilon_{278} = 2400\ M^{-1}\ cm^{-1}$; Kilhoffer et al., 1980) and the BCA protein assay (Pierce) using both bovine serum albumin and bovine testes calmodulin as standards. Absorbance measurements were made on a Varian-Cary 210 double-beam spectrophotometer.

Tb^{3+} Luminescence Measurements. Fluorescence emission data were measured on a Perkin-Elmer MPF-44A spectrofluorometer equipped with a differential corrected spectra unit. Tyr138 was excited at 278 nm while its emission was scanned from 280 to 450 nm. Tyrosine-sensitized Tb^{3+} emission data were recorded by exciting Tyr138 at 278 nm and monitoring the Tb^{3+} emission at 545 nm. A 310-nm excitation filter was used to avoid intensity due to harmonic doubling. Excited-state lifetimes of Tb^{3+} bound to calmodulin were measured on a Photon Technology International Model LS100 pulsed fluorometer using the conditions described above for measurement of sensitized emission. A 5-nm slit width for both excitation and emission was used in all cases. Excited-state lifetime data were analyzed on a microcomputer using the commercially available program NFIT (Island Products) which employs the Marquardt–Levenberg nonlinear least-squares algorithm.

Eu^{3+} Luminescence Titrations. A Nd:YAG (Continuum series YG518C) pumped tunable dye laser (Model TDL50) pulsed at 10 Hz was used to obtain the excitation spectra and lifetime data. The details of this system are presented elsewhere (Tingey, 1987). A mixture of Rhodamine 590 (Exciton) and Rhodamine 610 (Kodak) dyes was used to excite the $^7F_0 \rightarrow {}^5D_0$ transition (578–581 nm) of the Eu^{3+} ion, while Coumarin 480 and 485 dyes (Exciton) were used to excite the $^7F_0 \rightarrow {}^5D_2$ (464–467 nm) and $^7F_0 \rightarrow {}^5D_1$ (524–527 nm) transitions, respectively. In each case, the $^5D_0 \rightarrow {}^7F_2$ emission was monitored at 614 nm. In the non-time-resolved experiments, intensities were collected in 10- or 20-s channels in a signal averager for 5–10 min. The resulting 30–35 channels were averaged to obtain a single intensity value which was then corrected for laser power fluctuations and sample dilution. For time-resolved experiments, luminescence decays were collected for a set time (4–8 min; 2400–4800 transients) and corrected for laser power fluctuations during the course of the experiment. The decays were analyzed into a sum of component exponential functions using the program LIFETIME (McNemar, 1988) which is also based on the nonlinear regression method developed by Marquardt (1963). The quality of the fit was judged by plots of the weighted residuals of a fit of the data; symmetric deviations from zero were taken as evidence of a good fit.

Ln^{3+}–CaM Binding Constant Measurements. Binding curves for Eu^{3+} and Tb^{3+} were obtained using the non-time-resolved methodology described above. Binding constant measurements for the tight Ln^{3+} sites (I and II) were determined using 50 nM protein samples. Experiments to determine the binding constant for the weak Ln^{3+} sites (III and IV) were conducted at protein concentrations of 10–15 μM. In analyzing the data for sites III and IV, the intensity at 2 equiv was subtracted from the subsequently acquired data in order to approximate the shape of the curve for these two sites alone. The binding curves used to fit the titration data were calculated using Newton's method for nonlinear systems (Feldman et al., 1972) and the assumption that the metal ion binding sites are independent. Errors reported for the K_d measurements represent the RMS deviation for three trials.

Metal Ion Competition Experiments. Competition experiments between Eu^{3+} and Ca^{2+} for sites I and II of CaM were conducted using the non-time-resolved methodology described above. Two equivalents of Eu^{3+} was added to a 50 nM protein solution buffered in D_2O; metal ion binding was allowed to equilibrate for at least 160 min prior to the measurement of the signal intensity arising from Eu^{3+} bound to the protein with excitation at 579.25 nm. Ca^{2+} was then added to the solution at total concentrations of 0.25, 0.50, and 1.0 mM, and the excitation intensity of the $^7F_0 \rightarrow {}^5D_0$ transition of the Eu^{3+} ion was measured after each addition. It was found necessary to allow a 90-min equilibration period after each Ca^{2+} addition before the luminescence intensity was recorded. Experiments were also conducted under conditions where the Ca^{2+} was added to the protein solution prior to the addition of 2 equiv of Eu^{3+}. The error in determining the apparent K_d for Ca^{2+} binding is reported as the RMS deviation for five trials.

Förster Energy-Transfer Parameters. Tyrosine fluorescence and Tb^{3+} absorption spectra were manually digitized using a Summagraphics MM1200 Series digitizing tablet. Overlap integrals, J, and critical distances for 50% energy transfer, R_0, were calculated from the program FREQLAP (C. W. McNemar and S. T. Frey, this laboratory). All programs developed in this laboratory were written in BASIC for the IBM CS9000 computer. Values for κ^2 were calculated from X-ray crystal structure coordinates (Protein Data Bank entry 3CLN; Babu et al., 1988), using the methodology outlined below. The effect of thermal motion on the calculated value of κ^2 was investigated by carrying out molecular dynamics simulations using the CHARMm molecular mechanics/dynamics package (Brooks et al., 1983) and determining the average κ^2 value from the resulting trajectory. The effects of solvent on side-chain motion were taken into account by including a 15-Å sphere of water molecules centered at the C_α of Tyr138. The water molecules were restrained inside the sphere by imposing a stochastic boundary potential (Brooks & Karplus, 1983); the portion of the protein outside of the sphere was held fixed. The crystallographic structure was taken as the starting point for the simulation, including calcium ions at sites III and IV. (It should be noted that both ions fell inside the mobile region defined by the 15-Å sphere.) Values for ϵ (–0.100) and $^1/_2R_{min}$ (1.60) for the calcium ions were determined by Horrocks (unpublished data). The simulation was carried out at 300 K using Langevin dynamics with 10 ps of equilibration and an additional 10-ps simulation period during which atomic coordinates were calculated in 1-fs steps and saved at 50-fs intervals. The coordinate sets saved in the second 10-ps frame were then used to compute averages and RMS deviations for κ^2.

At any given step, the value for κ^2 for an isotropic acceptor such as Tb^{3+} is given by

$$\kappa^2 = (1/3)(1 + 3\cos^2\theta) \quad (1)$$

(Dale & Eisenger, 1974) where θ is the angle between the donor emission vector and the distance vector between the donor (tyrosine) and the acceptor (Tb^{3+}). $\cos\theta$ is described by the normalized dot product of the emission and distance vectors. Substituting in eq 1 yields

$$\kappa^2 = (1/3)\{1 + 3[(\mathbf{D}\cdot\mathbf{R})^2]\} \quad (2)$$

where $\mathbf{R}$ is the donor–acceptor distance unit vector defined by

$$\mathbf{R} = \frac{\mathbf{r}_M - \mathbf{r}_{mid}}{|\mathbf{r}_M - \mathbf{r}_{mid}|} \quad (3)$$

with $\mathbf{r}_M$ describing the position of the metal ion and $\mathbf{r}_{mid}$ designating the location of the ring midpoint:

$$\mathbf{r}_{mid} = (\mathbf{r}_{C\gamma} + \mathbf{r}_{C\delta1} + \mathbf{r}_{C\delta2} + \mathbf{r}_{C\epsilon1} + \mathbf{r}_{C\epsilon2} + \mathbf{r}_{C\zeta})/6 \quad (4)$$

The tyrosine emission vector is polarized perpendicular to the C_2 axis and lies in the plane of the tyrosine ring (Jaffé & Orchin, 1962; Sponer, 1942). Therefore, $\mathbf{D}$, the unit vector which is normal to the C_γ–C_ζ tyrosine ring axis and lies in the plane of the ring, is given by

$$\mathbf{D} = \mathbf{d}/|\mathbf{d}| \quad (5)$$

where

$$\mathbf{d} = (\mathbf{r}_{C\epsilon1} - \mathbf{r}_{mid}) - \left\{\left[(\mathbf{r}_{C\epsilon1} - \mathbf{r}_{mid})\cdot\frac{\mathbf{r}_{C\gamma} - \mathbf{r}_{C\zeta}}{|\mathbf{r}_{C\gamma} - \mathbf{r}_{C\zeta}|}\right]\left(\frac{\mathbf{r}_{C\gamma} - \mathbf{r}_{C\zeta}}{|\mathbf{r}_{C\gamma} - \mathbf{r}_{C\zeta}|}\right)\right\} \quad (6)$$

Equations 5 and 6 represent the Schmidt orthonormalization of vectors $\mathbf{r}_{C\epsilon1} - \mathbf{r}_{mid}$ and $\mathbf{r}_{C\gamma} - \mathbf{r}_{C\zeta}$.

The computation of κ^2 for each step of the dynamics run was carried out by the combination of a CHARMm stream file which extracted the necessary coordinates from each trajectory frame and a custom FORTRAN program which read the coordinate sets and accumulated the desired averages and RMS deviations. All calculations were conducted on an IBM RISC System/6000.

RESULTS

Excitation Spectroscopy of the $^7F_0 \rightarrow {}^5D_0$, $^7F_0 \rightarrow {}^5D_1$, and $^7F_0 \rightarrow {}^5D_2$ Transitions of Eu^{3+}. An examination of the excitation spectroscopy of the $^7F_0 \rightarrow {}^5D_0$ transition of Eu^{3+} bound to octopus calmodulin (Figure 1) supports the idea that the minor differences in the amino acid sequences of octopus and mammalian calmodulin do not significantly affect the metal ion binding sites. The excitation spectra reveal a broad band whose intensity increases as Eu^{3+} is added to the apoprotein, but whose shape varies little throughout the titration. There is a slight shift in the position of the peak maximum from 579.25 to 579.32 nm, while a shoulder at ~579.6 nm becomes apparent after 2 equiv of Eu^{3+} has been added. The wavelength of the excitation maximum (579.32 nm) corresponds to a total ligand charge of –2.7 surrounding the bound Eu^{3+} ions, according to the relationship established by Albin and Horrocks (1985). This result is consistent with the X-ray crystal structure (Babu et al., 1988, 1985), which indicates that three of the four metal binding sites (II, III, IV) contain three carboxylic acid ligands, while the remaining site (I) has four.

The excitation band was decomposed into component peaks using the program SPECTRUM (McNemar & Horrocks, 1989); the best fits were obtained using a combined Lorentzian–Gaussian lineshape function (Figure 1). Because neither the $^7F_0$ (ground) nor the $^5D_0$ (excited) state is split by the ligand field, each distinct Eu^{3+} environment will be represented by a single peak. However, it was not possible to resolve the broad OCaM excitation band (fwhm = 14 cm^{-1}) into the four peaks that might be expected. The three peaks identified in Figure 1 represent the best fit of the data as judged by plots of the weighted residuals and minimization of χ^2. Prior to the addition of 2 equiv of Eu^{3+}, a good fit is achieved with only two Lorenztian–Gaussian functions. In an earlier study of bovine testes calmodulin, Horrocks and Tingey (1988) reported a single peak for Eu^{3+} bound to the high-affinity sites (I and II) based on time-resolution of only a single exponential for 16 excitation wavelengths in the $^7F_0 \rightarrow {}^5D_0$ transition region (578.5–580.0 nm). Computer-aided deconvolution of a virtually continuous curve with 300 data points in the excitation

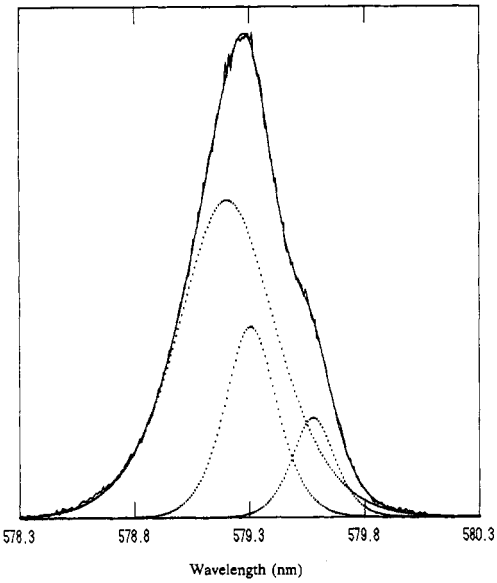

FIGURE 1: Curve-resolved $^7F_0 \rightarrow {}^5D_0$ excitation spectrum of 4 equiv of Eu^{3+} bound to OCaM (10 μM). The parameters of the fit are as follows: λ_1 = 579.21 nm, σ_1 = 0.50 nm; λ_2 = 579.31 nm, σ_2 = 0.27 nm; λ_3 = 579.58 nm, σ_3 = 0.22 nm, where λ is the wavelength of the peak maximum and σ is the full width at half-maximum intensity.

spectrum allows us to identify 2 distinct bands, which is not possible with a time-resolved spectrum consisting of a limited number of data points. We assign the species with an excitation maximum at 579.31 nm to Eu^{3+} binding at either site I or site II, due to its presence before more than 2 equiv of Eu^{3+} has been added. The most prominent component of the spectrum (579.21 nm) arises from the combination of intensity from both a high- and a low-affinity site, which we are unable to decompose further because of the apparent breadth of each band. However, for BCaM, the two component functions can be separated in the temporal mode as the excited-state lifetime values are quite different (2.40 and 1.70 ms in D_2O solution). The peak at 579.58 nm which appears only after 2 equiv of Eu^{3+} has been added to OCaM is attributed to Eu^{3+} binding to a low-affinity site (III or IV). Differences in the relative amplitudes of the component bands between the time-resolved (Horrocks & Tingey, 1988) and curve-resolved spectra are due to the dependence of the excitation spectrum on the quantum yields of the protein-bound Eu^{3+} ions in the various sites.

In contrast to the $^7F_0 \rightarrow {}^5D_0$ transition, excitation spectroscopy of the $^5D_1$ and $^5D_2$ states reveals details of the ligand field splittings of these levels, even when only a single metal ion environment is involved. For Eu^{3+} in a single, low-symmetry binding site, the $^5D_1$ and $^5D_2$ levels are expected to be split into three and five components, respectively. In general, our efforts to exploit the excitation of the $^7F_0 \rightarrow {}^5D_1$ level have not been successful due to poor signal intensity and lack of resolution. However, Figure 2 shows the band structure obtained when the $^7F_0 \rightarrow {}^5D_2$ transition (464–467 nm) is excited. The molar absorptivity of this transition is greater than that for the $^7F_0 \rightarrow {}^5D_0$ transition (0.1 vs 0.01 M^{-1} cm^{-1}). Consequently, it is easier to observe the ligand field splitting and to resolve spectrally the individual sites via direct methods. No significant changes in the excitation spectrum are observed until after 2 equiv of Eu^{3+} has been added to apo-OCaM. Subsequent additions of the metal ion produce dramatic changes in the overall shape of the spectrum. In Figure 2, trace A is representative of the spectrum obtained when 2 equiv of Eu^{3+} is bound to the Ln^{3+} ion high-affinity sites in the protein, while trace B shows the spectrum obtained when all four sites are occupied with metal (6 equiv of Eu^{3+} added).

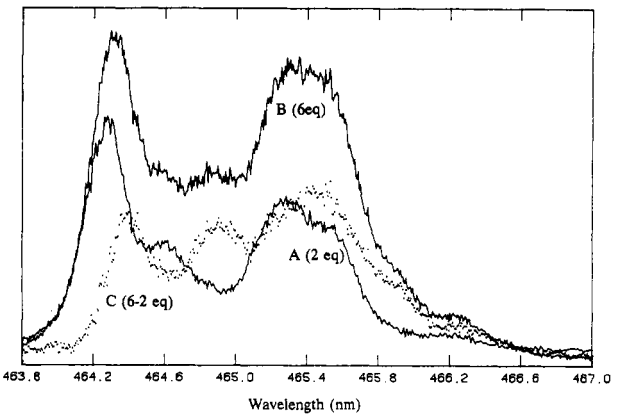

FIGURE 2: $^7F_0 \rightarrow {}^5D_2$ excitation spectrum (λ_{em} = 614 nm) of Eu^{3+} bound to OCaM (10 μM). (A) 2 equiv; (B) 6 equiv; (C) 6 – 2 equiv (···).

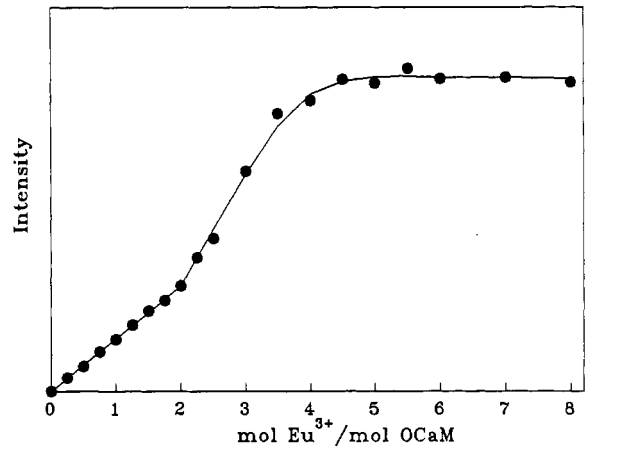

FIGURE 3: Intensity of the $^7F_0 \rightarrow {}^5D_0$ (λ_{ex} = 579.28 nm) excitation band as a function of total equivalents of Eu^{3+} added to apo-OCaM (10 μM). The solid line represents the theoretical fit of the data with K_d = 1.0 ± 0.2 μM.

Subtracting trace A from trace B yields trace C which represents the spectrum for occupation of the two weaker sites alone. This type of analysis allows us to assign regions of the spectrum to each set of sites and, through careful selection of the excitation wavelength, examine the sites individually. The difference spectrum indicates that a laser wavelength of 464.2 nm will excite ions in the tight sites predominantly; filling of the lower affinity sites can be best observed with excitation at 464.4, 464.9, or 465.4 nm. The $^7F_0 \rightarrow {}^5D_2$ excitation spectra observed for OCaM at various Eu^{3+}/OCaM ratios agree well with those recorded for BCaM (Mulqueen et al., 1985), thus indicating that the ligand field surrounding each Eu^{3+} ion is very similar for both proteins.

Non-Time-Resolved Experiments: Binding Constant Measurements for Tight and Weak Ln^{3+} Sites. For non-time-resolved experiments where signal intensity is collected using a single excitation wavelength, the intensity is proportional to the concentration of Eu^{3+} species contributing at that wavelength. Figure 3 shows the result of a titration of apo-OCaM with Eu^{3+} monitored with excitation of the $^7F_0 \rightarrow {}^5D_0$ band at 579.28 nm. The data indicate that two metal ions bind initially to the tight lanthanide binding sites (I and II) followed by binding to the lower affinity sites (III and IV). Using just the data for the two lower affinity sites and assuming two independent, equivalent sites, a dissociation constant of 1.0 ± 0.2 μM is calculated for the titration curve. The solid line represents the theoretical curve calculated to fit the data. The excitation wavelength was chosen to maximize intensity

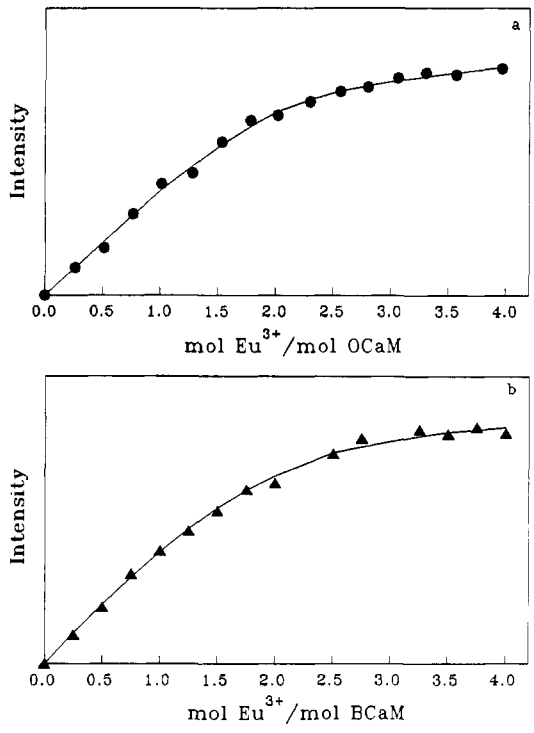

FIGURE 4: Eu^{3+} ion binding to the tight Ln^{3+} sites (I and II). Intensity of the $^7F_0 \rightarrow {}^5D_0$ (λ_{ex} = 579.25 nm) excitation band as a function of total equivalents of Eu^{3+} added to (a) OCaM (50 nM) and (b) BCaM (50 nM). The solid line represents the theoretical fit of the data with K_d = 6 ± 2 nM for OCaM and K_d = 12 ± 2 nM for BCaM.

contributions from Eu^{3+} ions bound at sites III and IV.

By going to much lower protein concentrations, where only sites I and II bind, it is possible to measure the dissociation constant for the tighter sites, which correspond to the straight-line portion of the titration curve shown in Figure 3. By taking advantage of the higher quantum yield of the Eu^{3+} ion in D_2O solution, it is possible to measure the signal intensity from Eu^{3+} bound to 50 nM OCaM. On the basis of excited-state lifetime data (see below), we found that the weak Ln^{3+} sites (III and IV) bind the Eu^{3+} ion upon initial addition, but upon equilibration over time these ions migrate to the tight sites (I and II) where they remain bound. Therefore, in order to prevent significant contributions to the signal intensity from sites III and IV, it was necessary to wait 20 min between the addition of each aliquot of Eu^{3+} and the measurement of bound Eu^{3+} luminescence intensity during the course of a titration (Figure 4a). Absence of Eu^{3+} ion binding to the weaker sites was verified by recording the excited-state lifetime after 4 equiv of Eu^{3+} had been added; only a single exponential was found with τ = 2.45 ms, corresponding to that for sites I and II. The absence of a shoulder at ~579.6 nm in the excitation spectrum also indicates that under these conditions the binding is solely at sites I and II. Assuming two independent, equivalent sites, a dissociation constant of 6 ± 2 nM is calculated for the tight Ln^{3+} sites of the OCaM protein. To complete our comparison between the bovine testes and octopus calmodulin isotypes, an analogous experiment was carried out for the mammalian protein. The solid line in Figure 4b is the theoretical curve calculated to fit the data with K_d = 12 ± 2 nM.

Effective K_d Measurement for Ca^{2+} Binding to Sites I and II. Work conducted previously in this laboratory has demonstrated the usefulness of metal ion competition experiments in determining the effective metal ion dissociation constants for both multidentate ligands (Albin et al., 1984) and protein systems (Burroughs et al., 1992; Breen et al., 1985) provided the dissociation constant for Eu^{3+} is known. In these experiments, the intensity of the $^7F_0 \rightarrow {}^5D_0$ transition of the Eu^{3+}–ligand complex is compared in the presence and absence of a competing metal ion. The amount by which the Eu^{3+}–ligand signal intensity is reduced is directly proportional to the amount of Eu^{3+} that has been replaced, thus making determination of relative binding constants possible. Competition experiments between Eu^{3+} and Ca^{2+} were performed in order to measure the relative affinity of calmodulin for Ca^{2+} in sites I and II. The conditions employed were based on the results of the K_d measurements for sites I and II as described above. The two tight Ln^{3+} sites (weak Ca^{2+} sites) were assumed to be equal and independent so that the metal ion competition can be described simply as involving a single site according to

$$Ca^{2+} + EuCaM \rightleftarrows Eu^{3+} + CaCaM \qquad (7)$$

where the equilibrium constant, K, for the above reaction is given by

$$K = \frac{K_{d(Eu)}}{K_{d(Ca)}} = \frac{[Eu^{3+}][CaCaM]}{[Ca^{2+}][EuCaM]} = \frac{([Eu^{3+}]_t - \alpha I')(I - I')}{[[Ca^{2+}]_t - \alpha(I - I')]I'} \qquad (8)$$

where I and I' are the $^7F_0 \rightarrow {}^5D_0$ excitation spectral intensities in the absence and presence of Ca^{2+}, respectively, α is the known proportionality constant between the intensity and the concentration of bound Eu^{3+}, and the subscript t denotes the total metal ion concentrations. Using the K_d measured for Eu^{3+} binding to the tight Ln^{3+} sites, the Ca^{2+} dissociation constant was found to be 26 ± 3 μM.

Time-Resolved Studies of Octopus Calmodulin. Often the $^7F_0 \rightarrow {}^5D_0$ transition of Eu^{3+} is not resolvable into separate peaks for each Eu^{3+} environment in the frequency domain. This has led our laboratory to develop and exploit a time-resolution technique whereby the individual binding sites may be examined on the basis of their differing excited-state lifetimes (Horrocks & Tingey, 1988). This technique (see Materials and Methods) was utilized in determining the excited-state lifetimes of Eu^{3+} bound to OCaM in both H_2O and D_2O solution. Horrocks and Sudnick (1981) have shown that the number of water molecules, q, coordinated to Eu^{3+} is

$$q = 1.05(\tau^{-1}_{H_2O} - \tau^{-1}_{D_2O}) \qquad (9)$$

where τ^{-1} is the reciprocal of the excited-state lifetime (ms^{-1}) in the solvent indicated. For OCaM in D_2O solution, we measure three distinct τ^{-1} values, 0.41, 0.49, and 1.67 ms^{-1}, of which two agree with quantities measured for Eu^{3+} ions bound to BCaM (0.41, 1.67 ms^{-1}) and one is slightly different (0.59 ms^{-1} BCaM vs 0.49 ms^{-1} OCaM). In H_2O solution, three excited-state lifetimes are detected also with reciprocal lifetimes of 2.27, 2.56, and 3.85 ms^{-1}, in contrast to two values reported (Horrocks & Tingey, 1988) for the mammalian protein (2.44, 3.70 ms^{-1}). However, a careful reexamination of BCaM revealed three lifetimes there as well (2.27, 2.56, and 3.85 ms^{-1}). On the basis of the difference in the magnitude of the intensity at time zero (I_0) between the two lifetimes resolved for sites III and IV in H_2O and D_2O solution, we are able to match the pairs of lifetime values for determination of the number of water molecules bound to the Eu^{3+} ion at each site. These results lead to the conclusion that two water molecules are coordinated at each of the four Eu^{3+} ion binding sites in both OCaM and BCaM (Table I). The reported errors represent deviations associated with determination of the excited-state lifetime values; however, the largest source

Table I: Data for Determination of the Number of Water Molecules, q, Coordinated to the Eu^{3+} Ions Bound to Octopus Calmodulin

	D_2O		H_2O	
sites	τ (ms)	τ^{-1} (ms^{-1})	τ^{-1} (ms^{-1})	q
I and II	2.45 ± 0.05	0.41 ± 0.01	2.56 ± 0.06	2.3 ± 0.5
III or IV	2.05 ± 0.10	0.49 ± 0.02	2.27 ± 0.06	1.9 ● 0.5
III or IV	0.60 ± 0.08	1.67 ± 0.25	3.85 ± 0.30	2.3 ± 0.5

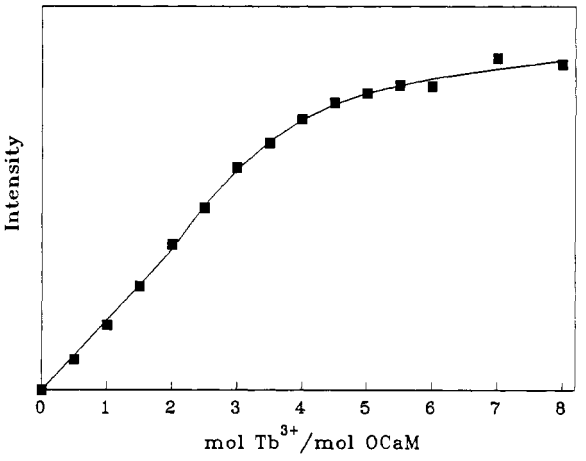

FIGURE 5: Intensity of the $^7F_6 \rightarrow {}^5D_4$ (λ_{ex} = 488 nm, λ_{em} = 545 nm) excitation band as a function of total equivalents of Tb^{3+} added to apo-OCaM (13 μM). The solid line represents the theoretical fit of the data with K_d = 5 ± 1 μM.

uncertainty stems from the empirical fit to the data used to determine eq 9 (Horrocks & Sudnick, 1981).

Intermetal Ion Distance Measurements from Förster-Type Nonradiative Energy Transfer. In addition to providing information regarding metal ion binding, time-resolved methods are also useful for structural characterization of protein systems. In an earlier study of bovine testes calmodulin, Horrocks and Tingey (1988) made use of Förster-type nonradiative energy transfer between excited Eu^{3+} ions and nearby Nd^{3+} ions bound at the four metal ion sites in the protein. The site–site distances obtained for each lobe of BCaM were in excellent agreement with those determined in the X-ray crystal structure (Babu et al., 1988). The same protocol is applied here to OCaM. Energy transfer is taken as intradomain and not interdomain due to the length of the central helix (~40 Å) and the r^{-6} distance dependence of Förster energy transfer. As show in this work, OCaM binds the first two added lanthanide ions quantitatively. Therefore, we can determine the distance between sites I and II by adding a total of 2 equiv of lanthanide ion to the protein in a 19:1 ratio of Nd^{3+} to Eu^{3+}. The excess of Nd^{3+} ensures that virtually every Eu^{3+} ion will have a Nd^{3+} neighbor. To obtain the distance between sites III and IV, a total of 4 equiv of lanthanide ion is added to the protein, again in a 19:1 ratio, and the data obtained at 2 equiv of lanthanide ion are subtracted. The resultant data are analyzed as a double exponential. The rationale used in the calculation has been set forth by Horrocks and Tingey (1988). In the calculation of R_0, the critical distance for 50% energy transfer, the overlap integral J was assumed to be the same as that for bovine testes calmodulin owing to the extreme similarity of their structures. The quantities and equations employed in the calculation, as well as the Eu^{3+} lifetimes in the absence (τ_0) and presence (τ_{Nd}) of energy transfer, are given in Table II. Uncertainty in the determined distances arises from previously outlined considerations of the quantum yield of the protein-bound Eu^{3+} ion (Horrocks & Tingey, 1988). The distances obtained for OCaM (12.4 ± 0.5 Å, sites I and II; 11.7 ± 0.8 Å, sites III and IV) agree well with those determined for BCaM (12.1 ± 0.5 Å, sites I and II; 11.6 ± 0.8 Å, sites III and IV), thereby affirming the similarity between the two isotypes. Excellent agreement is also obtained with the values determined from the crystal structure for the separation of the metal ion binding site pairs, 11.9 and 11.5 Å for the N-terminal and C-terminal lobes, respectively (Babu et al., 1988).

Binding of Tb^{3+} to Octopus Calmodulin: Laser Luminescence, Tyrosine Fluorescence, and Tyrosine-Sensitized Tb^{3+} Emission. There are several spectroscopic handles available to monitor the binding of Tb^{3+} ions to OCaM. For example, using 488-nm laser light, it is possible to excite the $^7F_6 \rightarrow {}^5D_4$ transition of the bound Tb^{3+} ion. When the emission intensity at 545 nm is monitored as function of Tb^{3+} added to apo-OCaM, the titration curve shown in Figure 5 is generated. These intensity data have been corrected for the presence of free Tb_{aq}^{3+} ion after 4 equiv of this ion has been added. The isotherm for Tb^{3+} binding to calmodulin closely matches that obtained in the Eu^{3+} non-time-resolved studies. The first two sites filled quantitatively, while the remaining two sites bind with a dissociation constant of 5 ± 1 μM. The slightly lower affinity of OCaM for Tb^{3+} than Eu^{3+} is consistent with earlier observations for BCaM (Mulqueen et al., 1985); the K_d value also agrees well with that determined by Wang and co-workers (6.7 μM; Wang et al., 1984).

The mammalian, piscine, and slime mold isotypes of calmodulin are unique in that they contain two tyrosine residues: one at position 99 in metal ion binding loop III and one at position 138 in binding loop IV. Most of the remaining isotypes possess only a single tyrosine residue in a position analogous to Tyr138. For vertebrate isotypes of calmodulin which contain two tyrosine residues, the fluorescence intensity of the tyrosine emission increases until 2 equiv of Tb^{3+} has been added, after which partial quenching of the tyrosine emission is observed, thus suggesting a global conformational change (Wang et al., 1982). The absence of Tyr99 in OCaM allows us to examine the metal ion binding and metal ion-induced structural changes which affect a single fluorophore. Figure 6 shows results of a titration of OCaM in which Tyr138 is excited at 278 nm and the emission is monitored at 306 nm as a function of added Tb^{3+}. The shape of the titration curve shows that the conformational changes induced by Tb^{3+} binding to OCaM are felt by the protein molecule when the first two metal ions bind, but are not complete until ~4 equiv of Tb^{3+} has been added. No quenching of the tyrosine emission is observed as a result of Tb^{3+} binding, thus indicating that the quenching observed for the two tyrosine isotypes of calmodulin involves changes in the environment of Tyr99 and not of Tyr138, an idea which was first suggested by Kilhoffer (1980). The effect of Tb^{3+} binding on tyrosine fluorescence contrasts with the changes produced by Ca^{2+} binding, which are complete after two Ca^{2+} ions have been added to the protein (Kilhoffer et al., 1980). However, CD investigations (Wang et al., 1984) and fluorescent probe studies (Tsuruta & Sano, 1990) indicate that structural changes in both lobes of the molecule are not complete until the protein binds four Ca^{2+} ions.

The examination of tyrosine-sensitized Tb^{3+} emission allows us to deduce the order of metal ion binding to OCaM. Sensitized emission of bound Tb^{3+} is observed at 545 nm as the protein is excited at 278 nm, in the region of maximal tyrosine absorption. This type of energy transfer between tyrosine and Tb^{3+} ions has been reported for both the BCaM (Mulqueen et al., 1985; Wang et al., 1982) and OCaM (Kilhoffer et al., 1980) isotypes. In the sensitized Tb^{3+} emission experiment conducted by Kilhoffer and co-workers, the Tb^{3+}

Table II: Parameters for Förster-Type Energy-Transfer Distance Measurements between Metal Sites of Octopus Calmodulin

sites	τ_0 (ms)	τ_{Nd} (ms)	E^a	ϕ^b	R_0 (Å)^{b,c}	r (Å)^d
I and II	2.45 ± 0.05	1.64 ± 0.05	0.331	0.70	11.0	12.4 ± 0.5
III and IV	2.05 ± 0.10	1.48 ± 0.10	0.278	0.39	10.0	11.7 ± 0.8
III and IV	0.60 ± 0.08	0.48 ± 0.08	0.200	0.25	9.3	11.7 ± 0.8

^{a} $E = 1 - \tau_{Nd}/\tau_0$. ^{b} Values taken from Horrocks and Tingey (1988). ^{c} $R_0^6 = (8.78 \times 10^{-25})\kappa^2\phi\eta^{-4}J$; $J = 1.4 \times 10^{-17}$ cm^6 mol^{-1}. ^{d} $r = R_0[(1-E)/E]^{-6}$.

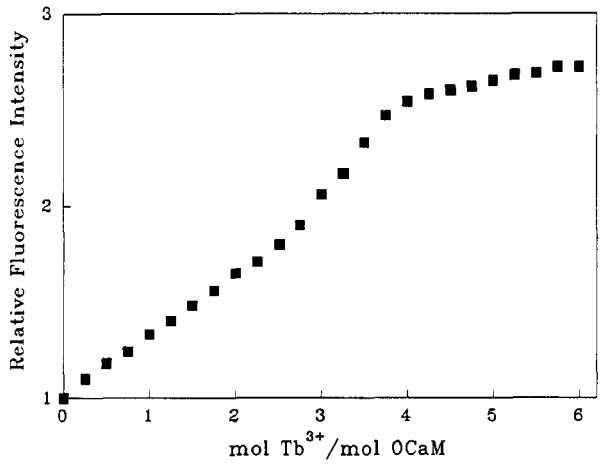

FIGURE 6: Relative fluorescence emission intensity of OCaM at 306 nm (λ_{ex} = 278 nm) as a function of total equivalents of Tb^{3+} added to apo-OCaM (19 μM).

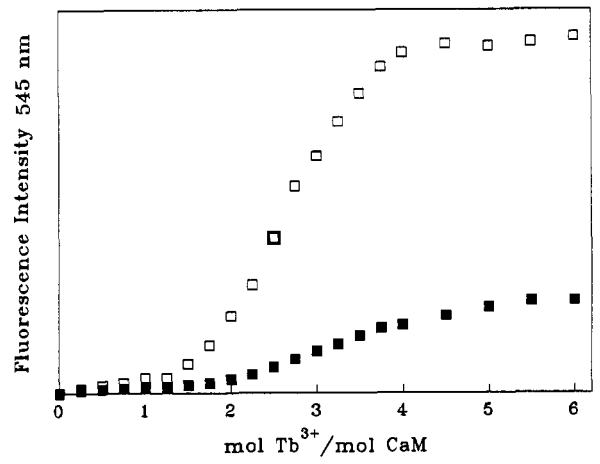

FIGURE 7: Tyrosine-sensitized Tb^{3+} emission at 545 nm (λ_{ex} = 278 nm) as a function of total equivalents of Tb^{3+} added to apo-OCaM (■, 25 μM) and BCaM (□, 30 μM). The fluorescence emission intensities have been scaled to account for the difference in protein concentration between the two experiments.

luminescence was reported to be negligible until almost 3 equiv of Tb^{3+} had been added to the protein. Further addition of Tb^{3+} caused a dramatic increase in the luminescence intensity which continued to rise even beyond the addition of 5 equiv of Tb^{3+}. We repeated this experiment for both OCaM and BCaM with the results shown in Figure 7. Our results are similar to those obtained in the earlier reported studies; however, we detect significant sensitized luminescence prior to the addition of 3 equiv of Tb^{3+} to OCaM, and see completion of Tb^{3+} binding upon the addition of 6 equiv of the metal ion. We attribute the discrepancy in the shape of the titration curves to the addition of salt (0.5 M KCl) in our experiments, which prevents Ln^{3+}-induced precipitation and, consequently, false luminescence intensity increases.

The results of the BCaM experiment (Figure 7, open squares) are included to show the significant increase in the magnitude of the observed sensitized emission intensity when Tyr99 is present. After 4 equiv of Tb^{3+} has been added, the observed sensitized Tb^{3+} emission signal is 5 times greater for BCaM than for OCaM. As indicated above, after 2 equiv of Tb^{3+} has been added to BCaM, a conformational change occurs which reduces the quantum yield of Tyr99. Using free tyrosine as the standard (ϕ = 0.14; Chen, 1967), we measured the quantum yield of Ln^{3+}-bound BCaM (ϕ_{BCaM} = 0.044) and estimate that the individual quantum yield of Tyr99 is reduced from 0.11 (Kilhoffer et al., 1981) in the Ca^{2+}-bound protein to 0.034 in the Tb^{3+}-bound form of the protein. Using distances (Tyr99→site III, IV ~ 7 Å) and values for the orientation factor κ^2 (Tyr99→site III = 0.47; Tyr99→site IV = 1.08) determined from the X-ray crystal structure (Babu et al., 1988), and applying Förster theory (Förster, 1948; see below), we calculate a ratio of 23 for the observed energy-transfer efficiency for BCaM relative to OCaM. The molar absorptivities reported for metal-bound BCaM (ϵ_{278} = 3000 M^{-1} cm^{-1}; Klee, 1977) and OCaM (ϵ_{278} = 2200 M^{-1} cm^{-1}; Seamon & Moore, 1980) suggest that Tyr99 and Tyr138 do not absorb 278-nm light equally. By assuming that Tyr99 has a molar absorptivity of 1500 M^{-1} cm^{-1} at 278 nm, the anticipated difference in the sensitized emission between BCaM and OCaM is reduced by a factor of 1.5 to yield 15. However, given the conformational change induced by Tb^{3+} binding, it is possible that the orientation factor and distances determined from the X-ray crystal structure of Ca^{2+}-bound CaM are different for Tb^{3+}-bound CaM, thus contributing to the discrepancy between the calculated and observed results.

Establishment of the Förster Mechanism for Energy Transfer between Tyrosine-138 and Tb^{3+} at Sites III and IV. The distance between an intrinsic protein fluorophore and bound Tb^{3+} ions can be determined from nonradiative energy-transfer measurements by application of the theory developed by Förster (1948). Horrocks and Collier (1981) established that energy transfer between a single tryptophan energy donor and two bound Tb^{3+} energy-acceptor ions occurs via the Förster mechanism in their study of cod III parvalbumin. The octopus calmodulin isotype, subject of the present study, represents a model for the investigation of the mechanism of energy transfer between a single tyrosine energy donor and Tb^{3+} energy-acceptor ions bound to sites III and IV of the protein.

According to Förster, the efficiency of energy transfer, E, between a single donor and a single acceptor is related to the actual distance of separation, r, and the critical distance for 50% energy transfer, R_0, by eq 10. R_0 is defined by eq 11,

$$E = [1 + (r/R_0)^6]^{-1} \quad (10)$$

$$R_0^6 = (8.78 \times 10^{-25})\kappa^2\phi_{Tyr}\eta^{-4}J \quad (11)$$

where κ^2 is the orientation factor, ϕ_{Tyr} is the quantum yield of the donor tyrosine in the absence of the acceptor, and η is the refractive index of the medium between the donor and acceptor. J is the spectral overlap integral defined by eq 12, where $F(\nu)$ is the fluorescence intensity of the donor and $\epsilon(\nu)$ is the molar absorptivity of the acceptor in units of M^{-1} cm^{-1}:

$$J = \frac{\int F(\nu)\epsilon(\nu)\nu^{-4}\,d\nu}{\int F(\nu)\,d\nu} \quad (12)$$

For the very low efficiencies that occur for Tyr→Tb^{3+} energy transfer, E is described by

$$E_{obsd} = \frac{A_{Tb^{3+}}}{A_{Tyr}}\frac{\phi_{Tyr}}{\phi_{Tb^{3+}}} \quad (13)$$

where $A_{Tb^{3+}}$ and A_{Tyr} are the integrated areas of the emission (cm^{-1} scale) for the acceptor (Tb^{3+}) and the donor (tyrosine) and ϕ_{Tyr} and $\phi_{Tb^{3+}}$ are the quantum yields of each species, respectively.

In order to improve the reliability of the distance calculation between the fluorophore and the bound metal ion, it is necessary to have as accurate knowledge as possible of the factors comprising R_0. The refractive index, η, is taken as 1.36, a value intermediate between that of water (1.34) and of organic molecules containing only first row atoms (1.39). Typically, the value for the orientation factor, κ^2, is taken as $^2/_3$, its value when both the donor and the acceptor are isotropic. While the Tb^{3+} ion, owing to the near-degeneracies of its excited levels, is a nearly isotropic acceptor, the transition dipole of the donor tyrosine ring emission is polarized. For the semi-isotropic case, the magnitude of κ^2 lies between $^1/_3$ and $^4/_3$ (Dale & Eisenger, 1974); however, in a single-donor, two-acceptor system, it is unlikely that the mean value of κ^2 will lie at either extreme. Therefore, using the isotropic value as an approximation for κ^2 should not introduce significant error into the determination of R_0. In fact, R_0 and consequently the derived distance r vary by only ± 12% if the minimum or maximum extremes of κ^2 are taken. The availability of the X-ray crystal structure coordinates for calmodulin (Babu et al., 1988) allows us to evaluate κ^2 in a more rigorous manner. Using the X-ray results and the fact that the emission dipole of tyrosine is polarized perpendicular to the C_2 axis of the phenol ring (Jaffé & Orchin, 1962; Sponer, 1942), values of $\kappa^2 = 0.68$ (Tyr138→Tb^{3+}, site III) and $\kappa^2 = 0.34$ (Tyr138→Tb^{3+}, site IV) were calculated as outlined under Materials and Methods. We investigated the effect of thermal motion on the κ^2 values. The average values for κ^2 are 0.76 ± 0.07 (Tyr138→Tb^{3+}, site III) and 0.35 ± 0.02 (Tyr138→Tb^{3+}, site IV).

An accurate determination of the magnitude of the spectral overlap integral, J, is perhaps the most critical factor in the determination of R_0. In principle, this quantity can be calculated from the donor (tyrosine) emission spectrum and the absorption spectrum of a bound Tb^{3+} ion in the wavelength region of tyrosine fluorescence. The emission from Tyr138 is easily recorded; however, the absorption spectrum of the acceptor Tb^{3+} bound to OCaM is unobtainable owing to the low molar absorptivity of the f–f transitions. For this reason, Tb^{3+} complexes of the polyaminocarboxylic acid ligands dtpa, hedta, ttha, and egta were used as models for the absorption of Tb^{3+} bound to the protein. The absorption spectrum of a 0.3 M solution of Tb(dtpa) reveals relatively sharp f–f transitions (Figure 8). The similarity in the absorption spectra of the various Tb^{3+} model complexes leads to a limited range of calculated J values [$(0.91–1.20) \times 10^{-19}$ cm^6 mol^{-1}; Table III] and suggests that the absorption spectrum of the protein-bound Tb^{3+} ion is likely to be similar to those of the models. The variation in J (±13%) represents ~2% difference in the calculated R_0 values, which further justifies the use of data from the model complexes in the evaluation of R_0.

The quantum yield of the energy donor (Tyr138) in the absence of the energy acceptor (Tb^{3+}) is required for the evaluation of R_0 (eq 11) and in the calculation of the efficiency of energy transfer (eq 13). Using the corrected emission spectrum of Tyr138 excited at 278 nm and free tyrosine as the standard ($\phi = 0.14$), the quantum yield of Tyr138 on OCaM was determined according to the method of Chen (1967). Quantum yields of 0.049 and 0.054 were measured for the Ca^{2+}- and Tb^{3+}-bound protein, respectively. Both values agree well with those reported previously (Kilhoffer et al., 1980). The quantum yield of the acceptor (Tb^{3+}) is also needed to determine the efficiency (eq 13); however, this is difficult to determine exactly owing to its weak absorption and the lack of an appropriate standard. An upper limit for $\phi_{Tb^{3+}}$ can be determined from the ratio of the excited-state lifetimes in H_2O and D_2O (Horrocks & Sudnick, 1981). The quantum yield of Tb^{3+} bound to OCaM was calculated ($\phi_{Tb^{3+}} = 0.48$) from excited-state lifetime values in H_2O ($\tau = 1.20$ ms) and D_2O ($\tau = 2.50$ ms), which were measured under the same conditions ($\lambda_{ex} = 278$ nm, $\lambda_{em} = 545$ nm) that the energy-transfer experiment was conducted.

With use of the quantities described above for the spectral overlap integral J, the quantum yield ϕ_{Tyr138} for the Tb^{3+}-bound protein, and the individual κ^2 values determined from the X-ray crystal structure, the following R_0 values were determined: Tyr138→Tb^{3+} at site III, 3.14 ± 0.06 Å; Tyr138→Tb^{3+} at site IV, 2.80 ± 0.06 Å. The uncertainties are the RMS deviations from the mean R_0 value and reflect the variation in the J values calculated for the different model complexes (Table III). Using an average value for the spectral overlap integral, $J = 1.00 \times 10^{-19}$ cm^6 mol^{-1}, R_0 was computed for each of the 200 coordinate sets saved during the 10 ps of dynamics, and averaged. The resultant values are quite similar to those calculated for the static structure and reflect only minor changes in κ^2 during the course of the dynamics

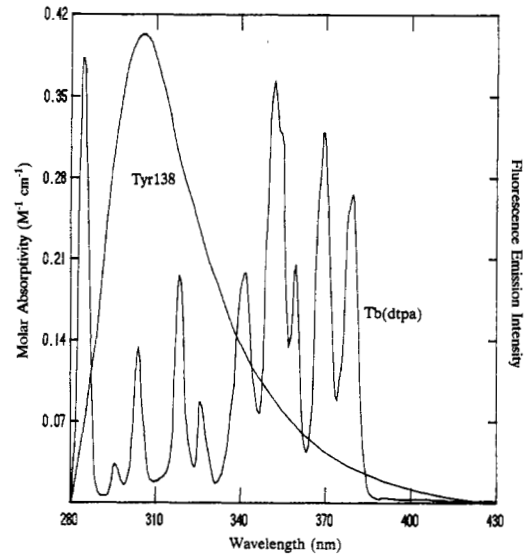

FIGURE 8: Overlap between the corrected fluorescence emission spectrum (λ_{ex} = 278 nm) of Tyr138 (donor) and the absorption spectrum of 0.3 M Tb(dtpa) (acceptor).

Table III: Energy-Transfer Parameters for Tb^{3+} Complexes of dtpa, hedta, ttha, and egta

acceptor	κ^2	J ($\times 10^{19}$ cm^6 mol^{-1})	R_0 (Å)
Tb(dtpa)	0.68	0.96	3.11
	0.34		2.77
Tb(hedta)	0.68	1.20	3.23
	0.34		2.86
Tb(ttha)	0.68	1.00	3.13
	0.34		2.79
Tb(egta)	0.68	0.91	3.08
	0.34		2.75

simulation. For Tyr138→Tb^{3+} at site III, R_0 is 3.20 ± 0.05 Å, and for Tyr138→Tb^{3+} at site IV, R_0 is 2.81 ± 0.02 Å.

The results of the tyrosine-sensitized Tb^{3+} emission experiment (Figure 7) indicate that energy is transferred from Tyr138 to protein-bound Tb^{3+} ions; however, the efficiency of energy transfer is so small that changes in the fluorescence emission intensity of Tyr138 are virtually unaffected by it. Therefore, in order to quantitate the energy transfer, the ratio of the fluorescence emission areas of the donor and acceptor (eq 13) was measured. For Tb^{3+} bound at sites III and IV of OCaM, the fluorescence emission bands at wavelengths other than 545 nm are poorly resolved, thus necessitating the use of polyaminocarboxylic acid complexes of Tb^{3+} to approximate the Tb^{3+} emission spectra. Because the relative intensities of the f–f emission bands vary little from system to system, we are able to scale the emission intensity of model complexes of Tb(dpa), Tb(edta), and Tb(hedta) to match the observed luminescence at 545 nm arising from protein-bound Tb^{3+} ions. Taking the experimentally determined value for $A_{Tb^{3+}}/A_{Tyr} = 3.41 \times 10^{-3}$ and values for $\phi_{Tyr138} = 0.054$ and $\phi_{Tb^{3+}} = 0.48$, one gets $E_{obsd} = 3.84 \times 10^{-4}$ (eq 13).

In cases of a single donor and two equivalent, equidistant acceptors, $E \approx E_{obsd}/2$, when E_{obsd} values are less than a few percent (Horrocks & Collier, 1981). The present analysis of energy transfer between Tyr138 and bound Tb^{3+} ions represents a single-donor, two-acceptor case where it is possible to partition the efficiency of energy transfer between the two acceptors. Using the individual R_0 values for each donor–acceptor pair, and the individual donor–acceptor distances from the X-ray crystal structure, we calculated a theoretical efficiency of energy transfer according to eq 10. Of the total predicted efficiency ($E = 3.05 \times 10^{-4}$), 60% arises from energy transfer between Tyr138 and Tb^{3+} at site III ($E_{III} = 1.83 \times 10^{-4}$), and 40% is from site IV ($E_{IV} = 1.22 \times 10^{-4}$), a distribution which is reasonably close to the $E \approx E_{obsd}/2$ approximation. The experimentally observed efficiency, E_{obsd}, was apportioned using the 60:40 ratio into the contributions for each site prior to computing the distance, r, between Tyr138 and Tb^{3+} at sites III and IV.

Verification that the Förster mechanism accounts for energy transfer between Tyr138 and protein-bound Tb^{3+} ions comes from the satisfactory agreement between distance estimates made from our measured energy-transfer efficiencies and calculated R_0 values, and the actual distances determined from the X-ray crystal structure. For Tyr138→Tb^{3+} at site III, taking $E_{III} = 2.30 \times 10^{-4}$ and $R_0 = 3.14$ Å, we calculate a distance r of 12.7 ± 0.2 Å. Similarly, taking $E_{IV} = 1.54 \times 10^{-4}$ and $R_0 = 2.80$ Å, we calculate a distance r of 12.1 ± 0.2 Å for Tyr138→Tb^{3+} at site IV. Both values are in good agreement with the distances determined from the static X-ray structure, 13.1 and 12.7 Å, for the phenol ring center of Tyr138 to Tb^{3+} at sites III and IV, respectively. The average distances between Tyr138 and the two Tb^{3+} ion sites, obtained from the dynamics run, are 13.5 ± 0.2 Å for Tyr138→Tb^{3+} at site III and 12.4 ± 0.2 Å for Tyr138→Tb^{3+} at site IV. Using the R_0 and distance values computed from the dynamics run, we reevaluated the expected energy-transfer efficiency (eq 10) and found that 57% of the energy transfer arises from Tyr138 and Tb^{3+} at site III while 43% is from Tb^{3+} to site IV. This minor change in the partitioning of the energy-transfer efficiency is expected given the small fluctuations in both R_0 and r during the dynamics simulation. By distributing the experimentally observed efficiency ($E_{obsd} = 3.84 \times 10^{-4}$) according to the 57:43 ratio, we calculate distances, r, of 13.0 and 12.0 Å for Tyr138 to sites III and IV, respectively, in very good agreement with the corresponding dynamically calculated distances of 13.5 and 12.4 Å.

DISCUSSION

Laser Experiments. While the previous Eu^{3+} ion luminescence studies (Horrocks & Tingey, 1988; Mulqueen et al., 1985) of the vertebrate calmodulin derived from bovine testes provided a complete picture of Eu^{3+} binding to calmodulin, the present experiments with the octopus calmodulin isotype attest to the extreme similarities of vertebrate and invertebrate calmodulin and provide additional quantitative information regarding metal ion binding to CaM. It is clear from Eu^{3+} spectroscopy that the minor differences in the amino acid sequence do not cause discernible differences in the metal ion binding sites between isotypes. Even substitutions at residues involved in metal ion binding (Asn60→Asp, site II; Asn97→Asp and Tyr99→Phe, site III; Asn129→Asp, site IV) do not produce significant differences in the appearance of the excitation spectra. The Eu^{3+} excited-state lifetime values for the two isotypes in H_2O solution are in good agreement; however, we do detect minor differences in these values for OCaM and BCaM in D_2O solution. Two of the three excited-state lifetimes measured for BCaM (2.40, 0.60 ms) are also observed for OCaM, while the third value is slightly different (1.70 vs 2.05 ms). The reciprocal of an observed lifetime, τ^{-1}, is comprised of radiative (k_{rad}) and nonradiative (k_{nonrad}) deexcitation rate constants. While both k_{rad} and k_{nonrad} are environmentally sensitive, k_{rad} is not sensitive to isotopic differences (H_2O vs D_2O). Therefore, since the difference in the Eu^{3+} excited-state lifetime belonging to either site III or site IV does not represent a change in the number of coordinated water molecules (see Table I), the longer lifetime in OCaM relative to BCaM must be attributed to some environmental factor which creates a less efficient deexcitation pathway in the invertebrate protein. We have examined the variations in the primary sequences of Ca^{2+} binding domains III and IV of BCaM and OCaM using the published sequences for both isotypes (Klee & Vanaman, 1982; Toda et al., 1981). In addition, we have begun recently a study of Eu^{3+} binding to a recombinant calmodulin from *Drosophila melanogaster* (DmCaM) which displays a 2.05-ms lifetime in D_2O (J. Bruno, unpublished results). DmCaM deviates from BCaM at four positions: Tyr99→Phe, Asn129→Asp, Gln143→Thr, and Ala147→Ser, all substitutions which also occur in OCaM. Comparison of OCaM with DmCaM allows us to rule out the Asn97→Asp substitution in site III as the cause of the anomalous excited-state lifetime value in OCaM as this mutation is not present in DmCaM. The recent report of the X-ray crystal structure of DmCaM (Taylor et al., 1991) is helpful in delineating the consequences of the other amino acid differences between OCaM and BCaM. It is unlikely that Asn129→Asp causes any effect on the excited-state lifetime value as the DmCaM static structure does not indicate any gross changes in the environment of the Asp129 side chain relative to Asn129 in the mammalian structure. Furthermore, the Asn→Asp change at position 60 in domain II does not cause any detectable change in the excited-state lifetime value corresponding to that site.

The Tyr99→Phe substitution in binding loop III, although spatially conservative, places a nonpolar phenylalanine residue in a highly exposed, polar (solvent) environment. Subtle structure changes which provide a more favorable locale for this residue could make the deexcitation of the Eu^{3+} ion excited state less efficient in invertebrate calmodulins. In support of this hypothesis, a comparison of the mammalian calmodulin

(Babu et al., 1988) and DmCaM (Taylor et al., 1991) X-ray crystal structures indicates that Phe99 is positioned ~1 Å closer to site IV than is Tyr99 in the mammalian structure.

The amino acids which make up binding loop IV are the same for both OCaM and BCaM. However, in OCaM, the substitutions Gln143→Thr and Ala147→Ser, just outside of loop IV, yield a hydrogen bond between the hydroxyl group of Ser147 and the carbonyl oxygen of Thr143. In addition, the X-ray structure of DmCaM (Taylor et al., 1991) indicates that the last three residues of the protein (Thr146 to C-terminus) form a loop, in contrast to the α-helix observed in the mammalian structure (Babu et al., 1988). Either one of these structural changes could provide a less efficient deexcitation pathway in OCaM. Currently we are investigating mutants of DmCaM in which the bidentate glutamic acid residue in each site has been changed to a noncoordinating residue in an attempt to destroy the metal binding capabilities of that site. Results of experiments with the mutant calmodulins may clarify the assignment and provide additional clues regarding excited-state deexcitation pathways inherent in protein systems.

Binding Constant Measurements. The dissociation constants determined for Eu^{3+} and Tb^{3+} at the weak Ln^{3+} ion binding sites (III and IV) in OCaM are in good agreement with those values determined for BCaM (Horrocks & Tingey, 1988; Mulqueen et al., 1985). The K_d values for Eu^{3+} ion dissociation from sites I and II are among the smallest values measured for a protein through a direct spectroscopic method. We measure a 100-fold difference in the affinity between the tight and weak sites for Eu^{3+}, a trend which mirrors the difference in Ca^{2+} ion affinities between the tight and weak sites for the native Ca^{2+} ion (Cox et al., 1988; Iida & Potter, 1986; Kilhoffer et al., 1983). It appears from these results that, regardless of the metal ion and the order of binding (N-terminal or C-terminal lobe first), two distinct classes of metal binding site exist for calmodulins from different sources.

Our ability to measure the apparent K_d for Eu^{3+} in the tight lanthanide sites (I and II) using our laser luminescence technique allows us to carry out competition experiments for the direct determination of the binding affinity of the native Ca^{2+} ion. Our experiments yield an effective K_d of 26 μM for Ca^{2+} binding to sites I and II of CaM. This value agrees well with that estimated by Wang (1985; 20 μM) in his theoretical model of the cooperativity of Ca^{2+} binding to CaM. However, it should be noted that the reported dissociation constants vary widely for the lower affinity Ca^{2+} ion binding sites [I and II; see Cox et al. (1988); Iida and Potter (1986), and Kilhoffer et al. (1983)]. Recently, Sellers and co-workers (Sellers et al., 1991) described the difficulty in reliably measuring Ca^{2+} binding constants due to metal ion-induced proton exchange and conformational changes, and the sensitivity to variations in temperature and ionic strength. Therefore, caution should be exercised when comparing binding data obtained under even slightly different experimental conditions.

Tyr→Tb^{3+} Energy Transfer via the Förster Mechanism. The availability of an appropriate model system and the X-ray crystal structure coordinates for calmodulin permits us to conduct the most thorough analysis of the Förster energy-transfer mechanism between an inherent protein chromophore (Tyr138) and a bound metal ion (Tb^{3+}) reported to date. Results of earlier investigations (Eberspach et al., 1988; Wallace et al., 1982) of Tyr→Tb^{3+} energy transfer suggested that Förster theory was valid for this donor–acceptor pair; however, limitations in each of those studies prevented unambiguous verification of the Förster mechanism.

In Förster energy-transfer studies between intrinsic protein fluorophores and protein-bound Tb^{3+} ions, the uncertainty in the value of the orientation factor κ^2 contributes to the error in the determination of R_0, the critical distance for 50% energy transfer. κ^2 is generally taken as $^2/_3$, a value midway between the two possible extremes ($^1/_3$ – $^4/_3$) for the semiisotropic case. Using the static crystal structure, we calculated values for the orientation factor which indicate that κ^2 values can approach one of the theoretical extremes ($\kappa^2 \approx {}^1/_3$, Tyr138→Tb^{3+} at site IV), but for the present single-donor, two-acceptor system, the mean value for κ^2 is reasonably close to $^2/_3$ ($\kappa^2_{avg} = 0.51$). Therefore, in a system for which the crystal structure is not available, satisfactory results may be obtained by using $\kappa^2 = {}^2/_3$. The excellent agreement between κ^2 values calculated from the X-ray structure and from the dynamics simulation encompassing Tyr138 and the metal ions at sites III and IV justifies the use of a static structure in the computation of the orientation factor, in the present case. It should be noted that Tyr138 is buried in a cluster of aromatic residues in the C-terminus and may be constrained to its crystallographic orientation through a hydrogen bond to Glu82 (Babu et al., 1988). In contrast, a more solvent-exposed tyrosyl residue, such as Tyr99 in BCaM, might be expected to show more variation in the range of possible κ^2 values. In the latter situation, the use of dynamics to evaluate κ^2 may be more realistic than employment of the static structure alone.

Incorrect evaluation of the spectral overlap integral J will also introduce error into the determination of R_0. In computing the overlap integral, it is important to include only absorption from the Tb^{3+} excited f-electron states and not background absorption from the ligand which will erroneously increase the calculated value of J. In our evaluation of the spectral overlap integrals, the absorption spectra of the polyaminocarboxylic acid complexes of Tb^{3+} were corrected for ligand absorption prior to the computation of the overlap between the donor (Tyr138) emission and the acceptor (Tb^{3+}) absorption. Uncorrected Tb^{3+} absorption spectra can yield J values which are 3 orders of magnitude too large, as demonstrated in the Tyr→Tb^{3+} energy-transfer studies conducted by Wallace et al. (1982) and Eberspach et al. (1988). Acceptable J values for a tyrosine donor and Tb^{3+} acceptor are on the order of 10^{-19} cm^6 mol^{-1}.

The efficiency of energy transfer between Tyr138 and Tb^{3+} ions bound at sites III and IV of OCaM is small; however, it yields a detectable Tb^{3+} fluorescence emission intensity which we are able to quantitate and apply in evaluating the Förster mechanism. The excellent agreement obtained between the distances calculated from our R_0 values and measured efficiencies, and distances from the X-ray structure (Babu et al., 1988), establishes that energy transfer between tyrosine and protein-bound Tb^{3+} ions occurs via the Förster mechanism. We examined the results of the distance calculation for Tyr138→Tb^{3+} at sites III and IV in which the mean value of κ^2 is taken as $^2/_3$ and the Tyr138 is assumed to be equidistant from the Tb^{3+} ions so that $E \approx E_{obsd}/2$. Using $E_{obsd} = 3.84 \times 10^{-4}$ and $R_0 = 3.13$ Å, the average distance, r, is 13.0 Å (eq 10). This value is in excellent agreement with an average distance, $r = 12.9$ Å, determined from the X-ray crystal structure. We provide this result as further proof that a Förster-type nonradiative mechanism effectively describes Try→Tb^{3+} energy transfer, and to justify the use of $\kappa^2 = {}^2/_3$ and $E \approx E_{obsd}/2$, in systems where a static structure is unavailable.

Conclusions. The sensitivity of the laser-induced lanthanide luminescence technique allows us to evaluate subtle effects caused by minor differences in the amino acid sequences

between calmodulin isotypes. We find that the differences in amino acid sequence between the vertebrate and invertebrate calmodulins studied have virtually no effect on their metal ion binding properties, and only minor effects on their luminescence properties.

Quantitation of the efficiency of energy transfer between Tyr138 and Tb^{3+} ions bound to OCaM proves that the luminescence transfer occurs via the Förster mechanism. The parameters of Förster theory established in this study of a tyrosine energy donor and Tb^{3+} energy-acceptor ions should form the basis for precise determinations of chromophore–metal ion distances in future studies of other proteins.

ACKNOWLEDGMENT

We thank Dr. Charles W. McNemar and Mr. Steven T. Frey for writing portions of the computer code used in this study and for many hours of helpful discussion. We are also grateful to Prof. J. J. Villafranca for generous use of his pulsed fluorometer to record the Tb^{3+} excited-state lifetime data and to Dr. J. S. Sack for providing the X-ray crystal structure coordinates for DmCaM.

REFERENCES

Albin, M., & Horrocks, W. DeW., Jr. (1985) *Inorg. Chem. 24*, 895–900.
Albin, M., Farber, G. K., & Horrocks, W. DeW., Jr. (1984) *Inorg. Chem. 23*, 1648–1651.
Andersson, A., Forsén, S., Thulin, E., & Vogel, H. J. (1983) *Biochemistry 22*, 2309–2313.
Babu, Y. S., Sack, J. S., Greenbough, T. J., Bugg, C. E., Means, A. R., & Cook, W. J. (1985) *Nature 315*, 37–40.
Babu, Y. S., Bugg, C. E., & Cook, W. J. (1988) *J. Mol. Biol. 254*, 191–204.
Breen, P. J., Hild, E. K., & Horrocks, W. DeW., Jr. (1985) *Biochemistry 24*, 4991–4997.
Brooks, B. R., Bruccoleri, R. E., Olafson, B. D., States, D. J., Swaminathan, S., & Karplus, M. (1983) *J. Comput. Chem. 4*, 187–217.
Brooks, C. L., & Karplus, M. (1983) *J. Chem. Phys. 79*, 6312–6325.
Buccigross, J. M., Chambers, V. L., & Boehnlein, J. A. (1989) *J. Less-Common Met. 149*, 213–218.
Burroughs, S. E., Eisenman, G., & Horrocks, W. DeW., Jr. (1992) *Biophys. Chem. 42*, 249–256.
Chao, S.-H., Suzuki, Y., Zysk, J. R., & Cheung, W. Y. (1984) *Mol. Pharmacol. 26*, 75–82.
Chen, R. F. (1967) *Anal. Lett. 1*, 35–42.
Cox, J. A., Comte, M., Mamar-Bachi, A., Milos, M., & Schaer, J.-J. (1988) in *Calcium and Calcium Binding Proteins* (Gerday, Ch., Bolis, L., & Gilles, R., Eds.) pp 141–162, Springer-Verlag, Berlin.
Crouch, T. H., & Klee, C. B. (1980) *Biochemistry 19*, 3692–3698.
Dale, R. E., & Eisenger, J. E. (1974) *Biopolymers 13*, 1573–1605.
Dedman, J. R., & Kaetzel, M. A. (1983) *Methods Enzymol. 102G*, 1–8.
De Moreno, M., Smith, J., & Smith, R. (1985) *Anal. Biochem. 151*, 466–470.
Eberspach, I., Strassburger, W., Glatter, V., Gerday, Ch., & Wollmer, A. (1988) *Biochim. Biophys. Acta 952*, 67–76.
Feldman, H., Rodbard, D., & Levine, D. (1972) *Anal. Biochem. 45*, 530–556.
Fritz, J. S., Oliver, R. T., & Pietrzyk, D. J. (1958) *Anal. Chem. 30*, 1111–1114.
Förster, T. (1948) *Ann. Phys. (Leipzig) 2*, 55–75.
Gerday, Ch., Bolis, L., & Gilles, R., Eds. (1988) *Calcium and Calcium Binding Proteins*, Springer-Verlag, Berlin.
Hidaka, H., Ed. (1989) *Adv. Exp. Med. Biol. 255*.
Horrocks, W. DeW., Jr. (1982) *Adv. Inorg. Biochem. 4*, 201–261.
Horrocks, W. DeW., Jr., & Collier, W. E. (1981) *J. Am. Chem. Soc. 103*, 2856–2862.
Horrocks, W. DeW., Jr., & Sudnick, D. R. (1981) *Acc. Chem. Res. 14*, 384–392.
Horrocks, W. DeW., Jr., & Tingey, J. M. (1988) *Biochemistry 27*, 413–419.
Iida, S., & Potter, J. D. (1986) *J. Biochem. 99*, 1765–1772.
Jaffé, H. H., & Orchin, M. (1962) *Theory and Applications of UV Spectroscopy*, John Wiley & Sons, New York.
Kilhoffer, M.-C., Gérard, D., & Demaille, J. G. (1980) *FEBS Lett. 120*, 99–103.
Kilhoffer, M.-C., Demaille, J. G., & Gérard, D. (1981) *Biochemistry 20*, 4407–4415.
Kilhoffer, M.-C., Haiech, J., & Demaille, J. G. (1983) *Mol. Cell. Biochem. 51*, 33–54.
Klee, C. B. (1977) *Biochemistry 16*, 1017–1024.
Klee, C. B., & Vanaman, T. C. (1982) *Adv. Protein Chem. 35*, 213–321.
Kretsinger, R. H. (1973) *Adv. Cyclic Nucleotide Res. 11*, 2–26.
Kumar, V. D., Lee, L., & Edwards, B. F. P. (1990) *Biochemistry 29*, 1404–1412.
Marquardt, D. W. (1963) *J. Soc. Ind. Appl. Math. 11*, 431–441.
Martin, S. R., Andersson Tellemann, A., Bayley, P. M., Drakenberg, T., & Forsén, S. (1985) *Eur. J. Biochem. 151*, 543–550.
McNemar, C. W. (1988) Ph.D. Thesis, The Pennsylvania State University, University Park, PA.
McNemar, C. W., & Horrocks, W. DeW., Jr. (1989) *Appl. Spectrosc.* 443, 816–821.
Moews, P. C., & Kretsinger, R. H. (1975) *J. Mol. Biol. 91*, 229–232.
Mulqueen, P., Tingey, J. M., & Horrocks, W. DeW., Jr. (1985) *Biochemistry 24*, 6639–6645.
Reuben, J. (1979) in *Handbook on the Physics and Chemistry of the Rare Earths* (Gschneider, K. A., & Eyring, L., Eds.) Vol. 3, pp 515–552, North-Holland, New York.
Seamon, K. B., & Moore, B. W. (1980) *J. Biol. Chem. 255*, 11644–11647.
Sellers, P., Laynez, J., Thulin, E., Forsén, S. (1991) *Biophys. Chem. 39*, 199–204.
Smith, V. L., Doyle, K. E., Maune, J. F., Munjaal, R. P., & Beckingham, K. (1987) *J. Mol. Biol. 196*, 471–485.
Sponer, H. (1942) *Rev. Mod. Phys. 14*, 224–231.
Taylor, D. A., Sack, J. S., Maune, J. F., Beckingham, K., & Quiocho, F. A. (1991) *J. Biol. Chem. 266*, 21375–21380.
Tingey, J. M. (1987) Ph.D. Thesis, The Pennsylvania State University, University Park, PA.
Toda, H., Yazawa, M., Kondo, K., Honma, T., Narita, K., & Yagi, K. (1981) *J. Biochem. 90*, 1493–1505.
Tsuruta, H., & Sano, T. (1990) *Biophys. Chem. 35*, 75–84.
Wallace, R. W., Tallant, E. A., Dockter, M. E., & Cheung, W. Y. (1982) *J. Biol. Chem. 257*, 1845–1854.
Wang, C.-L. A. (1985) *Biochem. Biophys. Res. Commun. 130*, 426–430.
Wang, C.-L. A., Aquaron, A. A., Leavis, P. C., & Gergely, J. (1982) *Eur. J. Biochem. 124*, 7–12.
Wang, C.-L. A., Leavis, P. C., & Gergely, J. (1984) *Biochemistry 23*, 6410–6415.